Received: 3 January 2017 | Revised: 21 March 2017 | Accepted: 26 March 2017

DOI: 10.1002/aoc.3851

FULL PAPER

WILEY Applied Organometallic Chemistry

Synthesis, crystal structure, DNA interaction and anticancer evaluation of pyruvic acid derived hydrazone and its transition metal complexes

Divya Hegde[1] | Suneel Dodamani[2] | Vijay Kumbar[2] | Sunil Jalalpure[2,3] | Kalagouda B. Gudasi[1]

[1] Department of Chemistry, Karnatak University, Pavate Nagar, Dharwad-580003, Karnataka, India

[2] Dr. Prabhakar Kore Basic Science Research Center, KLE University, Nehru Nagar, Belgaum-590010, Karnataka, India

[3] KLE University's College of Pharmacy, Nehru Nagar, Belgaum-590010, Karnataka, India

Correspondence
Kalagouda B. Gudasi, Department of Chemistry, Karnatak University, Pavate Nagar, Dharwad-580003, Karnataka, India.
Email: drkbgudasi@kud.ac.in

A novel tridentate chelating ligand, Ethyl 2-(2-(2-chlorobenzoyl)hydrazono) propanoate and its late transition metal complexes were synthesized, characterized and evaluated for anticancer behavior. The structures were elucidated with the help of elemental analyses, spectral (vibrational, electronic, NMR and mass) and thermo-gravimetric techniques. Single crystal X-ray crystallographic studies of the ligand suggest an orthorhombic lattice structure with *Pna21* space group. The interaction of ligand and complexes with DNA (CT-DNA) has been extensively studied using absorption, emission, viscosity and thermal denaturation studies with *E. coli* DNA. The DNA cleavage ability of ligand and metal complexes was tested using plasmid pBR322 DNA by gel electrophoresis method. The ligand and its copper complex have been evaluated for their *in vitro* anticancer activity against human cancer cells of different origin such as KB (Oral), A431 (Skin), Mia-Pa-Ca (Pancreases), K-549 (Lung), K-562 (Leukemia), MCF-7 (Breast) and VERO by MTT assay and the apoptosis assay was carried out with acridine orange/ethidium bromide (AO/EB) staining method. The studies suggest that ligand and copper complex exhibit significant cytotoxic activity on KB, MCF-7, A-431, Mia-Pa-Ca-2 an d A-549 cell lines compared to K-562 and VERO cell lines.

KEYWORDS
anticancer studies, DNA binding and cleavage studies, hydrazone, transition metal complexes, pyruvic acid

1 | INTRODUCTION

Cancer is a malignant disease responsible for high levels of mortality and morbidity throughout the world.[1,2] Chemotherapy is one of the most notable healing approaches. Numerous chemotherapeutic agents developed to date often failed, as drug-resistant tumour cells became predominant. But drug-based approaches for the cancer therapy are still among the most widely used methods due to the invention of new and better drugs.[3] Among them, simple benzoic acid derivatives, nitrogen and sulphur heterocycles, aliphatic carboxylic/pyruvic acid derivatives, Schiff bases, and many transition metal complexes have attracted much attention due to their promising cancer inhibiting properties.

Now a days researcher mainly focuses on simple drugs without or less side effects, cost effective and easy preparative methods.[4] Para-amino benzoic acid (PABA) is a water soluble naturally occurring compound and is essential for microorganisms and some animals. Few reports suggest that, PABA inhibit enzymes such as tyrosinase involved in melanogenesis, or bind to PXR (Pregnane X Receptor)/ SXR (Xenobiotic Sensing Nuclear Receptor) receptors to regulate genes involved in cell cycle progression.[5]

Accordingly, identification of lead compounds with these activities will likely lead to improved tumour specific treatment for numerous cancers including melanoma.[6] Structure–activity relationship study of a novel aspirin derivative shows strong anticancer activity.[7,8] A series of benzyl esters (ABEs) and their inhibitory activity against human colon (HT-29 and SW480) and pancreatic (BxPC-3 and MIA PaCa-2) cancer cell lines were evaluated. The benzyl esters bearing an aspirin or acyloxy group at the *meta* or *para* position of the benzyl ring have shown better activity.[9] It is proposed that, nature of the salicyloyl/acyloxy function, the leaving group, and the additional substituent, affecting the electron density of the benzyl ring, are influential determinants of the inhibitory activity on cancer cell growth.

Ethyl pyruvate/pyruvic acid and its derivatives have attracted much attention in anticancer research.[10,11] Preliminary evidence for the anti-inflammatory effects of ethyl pyruvate came from studies carried out by Yang *et al.* and Venkataraman *et al.*[6–11] They have demonstrated that resuscitation with a solution containing ethyl pyruvate down-regulated activation of the pro-inflammatory transcription factor, NF-kB, as well as the expression of several pro-inflammatory proteins, such as TNF, IL-6, cyclooxygenase (COX)-2, and inducible nitric oxide synthase (iNOS), in liver and intestinal mucosa.[6] The treatment with ethyl pyruvate/pyruvic acid has shown to improve survival and/or ameliorate organ dysfunction in a wide variety of preclinical models of critical illnesses, such as severe sepsis, acute respiratory distress syndrome, acute pancreatitis and stroke. Increasingly, however, it is becoming apparent that certain pyruvate esters have pharmacological effects, such as suppression of inflammation, that are quite distinct from those exerted by pyruvate anion.[11] Ethyl pyruvate (EP) also interfered with the angiogenic cascade, including growth, invasion, migration, and tube formation. Activation of NF-kB by vascular endothelial cell growth factor was reduced by ethyl pyruvate.[10] The data demonstrated that EP has a strong anti-angiogenic activity and may be useful as a multi-functional drug for treatment of variety of diseases, including inflammation, sepsis, hemorrhagic shock, coagulation, and ischemia/reperfusion, as well as diseases related to angiogenesis.

The synthesis of structurally related compounds may increase the anticancer activity drastically. Hence we designed new substituted benzoic acid and ethyl pyruvate based ligand and tested it for anticancer activity. The use of transition metal complexes for the treatment of cancer is known in medicinal field.[12–16] Considering this, transition metal complexes of the new ligand were synthesised, ligand and its copper complex were studied for their anticancer activity.

2 | EXPERIMENTAL

2.1 | Materials and methods

Ethyl pyruvate, tris-base, tris–HCl, calf thymus DNA and ethidium bromide (EB) were obtained from Sigma Aldrich and were of analytical grade. Hydrazine hydrate, 2-chlorobenzoic acid and metal chlorides are of AR grade and were obtained from Spectrochem, India. Plasmid DNA-pBR322 was purchased from Chromous Biotech, India. Agarose was obtained from Lonza (India). DMEM (Dulbecco's Modified Eagle's Medium) medium, FBS, fetal calf serum are purchased from Gibco, Thermofisher Scientific, Antibiotic-Antimycotic 100X solution and dual fluorescent staining solution AO/EB were purchased from Thermofisher Scientific. Oral cell line was purchased from NCCS Pune. All the solvents were of either HPLC or AR grade and obtained from S.D. Fine chemicals.

Metal content of Co(II), Ni(II) and Cu(II) complexes was determined volumetrically and while that of Zn(II) complex gravimetrically. Conductance measurements were recorded in DMF (10^{-3} M) using ELICO-CM-82 conductivity bridge with cell type CC-01 and cell constant 0.53. The IR spectra were recorded on a Nicolet 170SX FT-IR spectrometer with the fixed range of 4000–400 cm^{-1} using KBr disks. C, H, N were determined using Thermo quest elemental analyzer. ^{1}H and ^{13}C NMR spectra of ligand and zinc complex were recorded in DMSO-d_6 on a Bruker 500 MHz spectrometer. Electronic spectra were recorded on a Hitachi-U-3310 UV–visible spectrophotometer in the 200–1100 nm range using DMF (10^{-3} M) as the solvent. The fluorescence experiment was carried out on F-2500 spectrofluorometer (Hitachi, Japan) using 1.0 cm quartz cell. Thermogravimetric study was carried out over a temperature range of 25–800 °C using TGAQ500 analyzer with a heating rate of 10 °C min^{-1}.

2.2 | Synthesis

2.2.1 | Preparation of ligand [IV]

The ligand was synthesized in four simple steps as shown in Scheme 1. All the intermediates were characterised by NMR and GC mass analyses. Synthesis of the ligand involves following steps.

Synthesis of methyl-2-chlorobenzoate (II)

The desired ester (**II**) was prepared using literature procedure with slight modification.[17] To the methanolic solution of 2-chlorobenzoic acid (**I**) (15.60 g, 100 mM), a catalytic amount of conc.H_2SO_4 was added and refluxed for 10 hours. After completion of the reaction, methanol was evaporated and the resulting reaction mixture was extracted with ethyl acetate and organic layer was washed with sodium

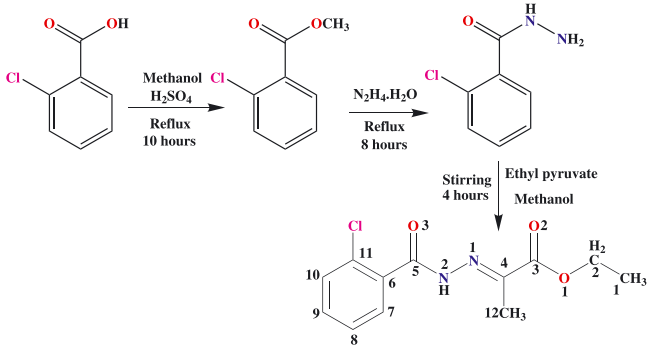

SCHEME 1 Synthetic route for ligand and its numbering scheme

bicarbonate, then with brine solution and dried over anhydrous magnesium sulphate. The solvent was removed *invacuo* to get the desired product. (Yield: 60%).

Synthesis of 2-Chlorobenzohydrazide (III)

To the methanolic solution of methyl-2-chlorobenzoate (9.38 g, 55 mM), hydrazine hydrate (8.25 g, 165 mM) was added slowly with stirring and refluxed for 8 hours. The hydrazide separated was filtered, washed with methanol and air dried. (Yield = 90%).

Synthesis of ethyl 2-(2-(2-chlorobenzoyl)hydrazono) propanoate (IV)

2-Chlorobenzohydrazide (8.36 g, 49 mM), ethyl pyruvate (5.68 g, 49 mM) in methanol (100 ml) was added and stirred for 4 hours. The white colored product obtained was washed thoroughly with cold methanol and air dried to get Ethyl 2-(2-(2-nitrobenzoyl)hydrazono)propanoate. The purity of the compound was checked by TLC on precoated silica gel plates (Rf: 0.45, Hexane: Ethyl acetate 3:7).

Yield 94%; m.p. 144–146 °C; white solid. Anal. Calcd for $C_{12}H_{13}ClN_2O_3$ (%): C, 53.64; H, 4.88; N, 10.43. Found (%): C, 53.61; H, 4.85; N, 10.43. IR (cm^{-1}): amide carbonyl ν(C5 = O3) 1692, pyruvate carbonyl ν(C3 = O2) 1717, azomethine ν(C = N) 1614. ^{1}H NMR (*E* and *Z* isomers) (500 MHz, DMSO-d_6, ppm): 11.21/11.47 (s, N2H, 1H), 1.26/1.04 (t, C1, 3H), 4.22/4.01 (q, C2, 2H). ^{13}C NMR (*E* and *Z* isomers) (500 MHz, DMSO-d_6, ppm): 170.38/170.32 (C3), 164.67/163.80 (C5), 134.94/135.48 (C4), 14.16/13.89 (C1), 61.30/60.82 (C2).

2.2.2 | General procedure for the synthesis of transition metal complexes

A suspension of ligand (0.50 g, 1.8 mM) in methanol (20 ml) was added to a methanolic solution of appropriate transition metal chlorides ($CoCl_2.6H_2O$, $NiCl_2.6H_2O$, $CuCl_2.2H_2O$ and $ZnCl_2$) in 1:1 molar ratio and refluxed for 7 hours. 2–3 drops of ammonia was added to the reaction mixture. The precipitate formed was filtered under reduced pressure, washed with methanol and air dried. All the complexes were obtained in good yields.

CoL. Yield 65%; Anal. Calcd for [Co($C_{20}H_{16}Cl_2N_4O_6$)].H_2O (%): C, 43.19; H, 3.26; N, 10.07; Co, 10.60. Found (%): C, 43.17; H, 3.24; N, 10.04; Co, 10.59. IR (cm^{-1}): amide carbonyl ν(C5 = O3) 1649, azomethine ν(C = N) 1570, ν_{asym}(C3O2O1) 1593, ν_{sym}(C3O2O1) 1376.

NiL. Yield 62%; Anal. Calcd for [Ni($C_{20}H_{16}Cl_2N_4O_6$)].H_2O (%): C, 43.21; H, 3.26; N, 10.08; Ni, 10.56. Found (%): C, 43.18; H, 3.24; N, 10.02; Ni, 10.55. IR (cm^{-1}): amide carbonyl ν(C5 = O3) 1620, azomethine ν(C = N) 1570, ν_{asym}(C3O2O1) 1592, ν_{sym}(C3O2O1) 1384.

CuL. Yield 70%; Anal. Calcd for [Cu($C_{20}H_{16}Cl_2N_4O_6$)].$2H_2O$ (%):C, 41.50; H, 3.48; N, 9.68; Cu, 10.98. Found (%): C, 41.51; H, 3.45; N, 9.64; Cu, 11.06. IR (cm^{-1}): amide carbonyl ν(C5 = O3) 1647, azomethine ν(C = N) 1583, ν_{asym}(C3O2O1) 1593, ν_{sym}(C3O2O1) 1383.

ZnL. Yield 61%; Anal. Calcd for [Zn($C_{20}H_{16}Cl_2N_4O_6$)].$2H_2O$ (%):C, 41.37; H, 3.47; N, 9.65; Zn, 11.26. Found (%): C, 41.39; H, 3.43; N, 9.67; Zn, 11.28. IR (cm^{-1}): amide carbonyl ν(C5 = O3) 1658, azomethine ν(C = N) 1597, ν_{asym}(C3O2O1) 1597, ν_{sym}(C3O2O1) 1361. ^{1}H NMR (500 MHz, DMSO-d_6, ppm): 11.20 (s, N2H, 1H). ^{13}C NMR (500 MHz, DMSO-d_6, ppm): 174.66 (C3), 166.81 (C5), 137.06 (C4).

2.3 | X-ray crystallography

Single crystal X-ray diffraction study of ethyl 2-(2-(2-chlorobenzoyl)hydrazono)propanoate was taken up at 296 K using BRUKER SMART APEX-CCD diffractometer with Mo Kα radiation (λ =0.71073). All the non-hydrogen atoms were refined with anisotropic temperature factors. The structures were solved using SHELXL-97 and refined using Full-matrix least squares F^2. All the calculations were performed using WinGX crystallographic software. Molecular geometry calculations were made using PARST and the structure drawing was obtained with ORTEP-3 for windows program.[18–20]

2.4 | Biological studies

The following biological studies have been undertaken to evaluate the activity of newly synthesized compounds.

2.4.1 | DNA binding studies

The interaction of the prepared compounds with DNA was evaluated extensively through different techniques.

UV absorption studies

UV Absorption experiments were performed by maintaining a constant ligand and metal complex concentration (20 μM)

and varying nucleotide concentration (0–60 μM) in buffer. The concentration of CT-DNA was calculated from its known extinction coefficient at 260 nm (6600 M^{-1} cm^{-1}). Solutions of calf thymus DNA in phosphate buffer gave a ratio of UV absorbance at 260 and 280 nm (A260/A280) 1.8–1.9, indicating that the DNA was pure and sufficiently free of contaminants like the proteins and RNA. The solution of DNA and desired compounds were kept to equilibrate at 25 °C for 20 min, after which absorption readings were noted. The data were then fit to following equation (1) to obtain intrinsic binding constant Kb.[21–23]

$$[DNA]/[\varepsilon_a-\varepsilon_f] = [DNA]/[\varepsilon_b-\varepsilon_f] + 1/Kb[\varepsilon_b-\varepsilon_f] \quad (1)$$

Where, [DNA] = concentration of DNA in base pairs,

ε_a is the extinction coefficient observed for the MLCT absorption band at the given DNA concentration,

ε_f is the extinction coefficient of the complex without DNA, and

ε_b is the extinction coefficient of the complex when fully bound to DNA.

A plot of $[DNA]/[\varepsilon_a-\varepsilon_f]$ v/s [DNA] gave a slope $1/[\varepsilon_a - \varepsilon_f]$ and intercept equal to $(1/Kb)[\varepsilon_b-\varepsilon_f]$. The intrinsic binding constant Kb is the ratio of slope to the intercept.

Viscosity measurements

Viscosity experiments were carried out using Ostwald microviscometer maintained at 26 °C in a thermostatic water bath. Flow time of solutions in phosphate buffer was recorded in triplicate and an average flow time was calculated. Data was presented as $(\eta/\eta^0)^{1/3}$ versus binding ratio, where η is the viscosity of CT-DNA in the presence of complex and η^0 is the viscosity of DNA alone.[21,22,24,25]

Thermal denaturation study

DNA melting experiments were carried out in phosphate buffer on a HITACHI U-3310 spectrophotometer equipped with a temperature-controlling programmer ETC-717 (5 °C). Solutions of *E. coli* DNA (*Escherichia coli* DNA) in phosphate buffer gave a ratio of UV absorbance at 260 and 280 nm (A260/A280) as 1.8–1.9, indicating that the DNA was pure and sufficiently free of contaminants like the proteins and RNA. UV melting profiles were obtained by scanning A260 absorbance monitored at a heating rate of 5 °C/min for solutions of *E. coli* DNA (100 μM) in the absence and presence of ligand and metal complexes (20 μM) from 25 to 85 °C. The melting temperature T_m, which is defined as the temperature where half of the total base pairs are unbound, was determined from the midpoint of the melting curves.[21,23,25]

Competitive binding fluorescence measurements

The apparent binding constants (Kapp) of the complexes were determined by fluorescence spectral technique using ethidium bromide (EtBr) bound CT-DNA solution in phosphate buffer. The changes in fluorescence intensities at 596 nm (546 nm excitation) of EtBr bound to DNA were recorded with an increasing amount of ligand and metal complex concentration. EtBr was non-emissive in phosphate buffer due to fluorescence quenching of the free EtBr by the solvent molecules. In the presence of DNA, EtBr showed enhanced emission intensity due to its intercalative binding to DNA. A competitive binding of copper complex to CT-DNA resulted in the displacement of the bound EtBr, decreasing its emission intensity.[23–25] Addition of a second DNA binding molecule would quench the EtBr emission by either replacing the DNA-bound EtBr (if it binds to DNA more strongly than EtBr) or accepting an excited state electron from EtBr. The apparent binding constant (Kapp) has been calculated from the equation (2).

$$K_{EtBr}[EtBr] = K_{app}[Compound] \quad (2)$$

where K[EtBr] is 1 x10^7 M^{-1} and the concentration of EtBr is 20 μM; [complex] is the concentration of the complex causing 50% reduction in the emission intensity of EtBr.

DNA cleavage studies

The DNA cleavage study of the synthesized compounds was determined by agarose gel electrophoresis using the *E.coli* pBR322 plasmid as a target. The synthesized compounds (100 μM) were dissolved in 6% DMSO (dimethylsulfoxide) and mixed with the target plasmid (1:1). The mixture was then incubated at 37 °C for 2 h. After the incubation period, the plasmid and the compound mixture was mixed with the tracking dye, bromophenol blue (1:1). It was then loaded into 1% agarose gel (containing 0.5 μg/mL ethidium bromide) wells along with two control wells, the first one with the untreated plasmid and the second one with the plasmid treated with DMSO solvent. Finally it was electrophoresed at a constant voltage of 50 V constant voltage for about 30 mins using Tris-EDTA (TAE) buffer (pH = 8.0).[22–25] The bands were visualized by UV light and photographed for analysis. The extent of cleavage of the supercoiled DNA was determined by measuring intensities of the bands using Molecular Imager Geldoc gel-XR imaging system (BIORAD).

Experimental procedure for MTT assay

The cytotoxicity is performed by 3-(4,5-dimethylthiazol-2-yl)-2,5-diphenyltetrazolium bromide (MTT) assay. This is a colorimetric assay that measures the reduction of yellow 3-(4,5-dimethythiazol-2-yl)-2,5-diphenyltetrazolium bromide by mitochondrial succinate dehydrogenase. The MTT enters the cells and passes into the mitochondria where it is reduced

to an insoluble, colored (dark purple) formazan product. The cells are then solubilized with an organic solvent (DMSO) and the released, solubilised formazan reagent is measured spectrophotometrically using ELISA. Since reduction of MTT can only occur in metabolically active cells the level of activity is a measure of the viability of the cells.

The cell lines were cultured in DMEM medium which was supplemented with 10% FBS and 1% Antibiotic-Antimycotic 100X solution. The cells were seeded at a density of approximately 5×10^3 cells/well in a 96-well flat-bottom micro plate and maintained at 37 °C in 95% humidity and 5% CO_2 for overnight. Different concentrations (200, 100, 50, 25, 12.5, 6.5, 3.125 µg/300 µl) of compounds were treated. The cells were incubated for another 72 hours. The cells in well were washed twice with phosphate buffer solution, and 20 µl of the MTT staining solution (5 mg/ml in phosphate buffer solution) was added to each well and plate was incubated at 37 °C. After 4 h, 100 µl of dimethylsulfoxide (DMSO) was added to each well to dissolve the formazan crystals, and absorbance was recorded at 570 nm using micro plate reader (ELISA reader).[26] The results are compared with that of Cisplatin used as reference drug against KB(Oral), A431(Skin), MIA-Pa-Ca (Pancreases), K-549 (Lung), K-562 (Leukemia), MCF-7(Breast) and VERO cell lines. The IC_{50} values were calculated using graph Pad Prism Version 5.1. The surviving cells and inhibiting cells are calculated by using following formula.

Surviving cells (%) = Mean OD of test compound /Mean OD of negative control ×100 Inhibiting cells (%) =100-surviving cells.

Dual Acridine orange/ethidium bromide (AO/EB) fluorescent staining

The cell line oral (KB) was further tested for its apoptotic behavior after showing cytotoxicity activity at desired concentration. The DMEM culture medium containing 10% fetal calf serum was added to each well of a 96-well plate (100 µl/well). Cells were added to a final concentration of 2×10^4/ml and the plates were incubated. The samples, ligand and copper complex treated cells are seeded in a 24-well plate after being cultured for 4 days, 20 µl of trypsin was added into each well. When cells had sloughed off, suspensions (25 µl) were transferred to glass slides. Dual fluorescent staining solution (1 µl) containing 100 µg/ml AO and 100 µg/ml EB (AO/EB) was added to each suspension and then covered with a coverslip. The morphology of apoptotic cells was observed and 260 cells were counted within 10 min using a fluorescent microscope (Carl Zeiss AxioVert S100). Dual acridine orange/ethidium bromide (AO/EB) staining method was done in triplicate.[27]

3 | RESULTS AND DISCUSSION

The newly synthesized ligand was characterized by elemental analysis, IR, ^{1}H NMR, ^{13}C NMR and 2D CH-COSY NMR spectral studies. The ligand is soluble in chloroform, hot methanol, DMF and DMSO, where as complexes are soluble in DMF and DMSO. All the complexes are non-hygroscopic and stable in both solid and solution phases at room temperature. Analytical data of all synthesised compounds (Table S1) is within the acceptable range and confirm their structure. The lower molar conductance values of all the complexes suggest their non-electrolytic nature. White crystals suitable for XRD studies were isolated by slow evaporation of methanolic solution of ligand. Attempts to grow single crystals of metal complexes were unsuccessful. However, the complexes were comprehensively characterized by various established physico-chemical techniques. The ligand has undergone hydrolysis and converted into its carboxylic acid in presence of metal salts *in-situ* and later formed the corresponding metal complexes.

TABLE 1 Crystal refinement data for ligand

CCDC no.	1479628
Empirical formula	$C_{12}H_{13}ClN_2O_3$
Formula weight	268.70
Temperature	296(2) K
Wavelength	0.71073 Å
Crystal system	Orthorhombic
Space group	*P n a 21*
Unit cell dimensions	a = 8.3158(3) Å α = 90° b = 8.5171(3) Å β = 90° c = 18.5995(7) Å γ = 90°
Volume	1317.34(8) Å^3
Z	4
Reflections collected	6142
Goodness-of-fit on F2	0.951
F(000)	564
Final R indices [1776 data; $I > 2\sigma(I)$]	R1 = 0.0370, wR2 = 0.1048
Final R indices all data	R1 = 0.0447, wR2 = 0.1116
Weighting scheme	$w = 1/[\sigma^2(F_o^2) + (0.0788P)^2 + 0.0494P]$, Where $P = (F_o^2 + 2F_c^2)/3$
Theta range for data collection	2.19 to 25.18°
Index ranges	-9 < =h < =9, −8 < =k < =10, −19 < =l < =22
Data / restraints / parameters	2097 / 1 / 165
Density (calculated)	1.360 Mg/cm^3

TABLE 2 Selective bond lengths (Å) for the ligand obtained by crystal structure

Atom label	Bond length	Atom label	Bond length	Atom label	Bond length
Cl1-C11	1.715	O1-C3	1.321	C4-C12	1.486
O1-C2	1.452	O2-C5	1.213	C6-C7	1.366
O3-C3	1.194	N1-C4	1.281	C3-C4	1.495
N1-N2	1.365	N2-C5	1.354	C5-C6	1.489
N2-H2	0.860	C1-C2	1.423	C6-C11	1.387

TABLE 3 Selective bond angles (°) for the ligand obtained by crystal structure

Atoms	Bond angle	Atoms	Bond angle	Atoms	Bond angle
C3-O1-C2	117.4	C5-N2-H2	120.7	O1-C3-C4	113.2
C5-N2-N1	118.6	C1-C2-O1	110.1	C9-C10-C11	119.4
N1-N2-H2	120.7	O1-C2-H2A	109.6	C11-C10-H10	120.3
O3-C3-C4	122.4	O1-C2-H2B	109.6	O2-C5-C6	122.9
C4-N1-N2	117.5	O3-C3-O1	124.4	O2-C5-N2	123.4
N1-C4-C12	127.1	N1-C4-C3	115.8	N2-C5-C6	113.6

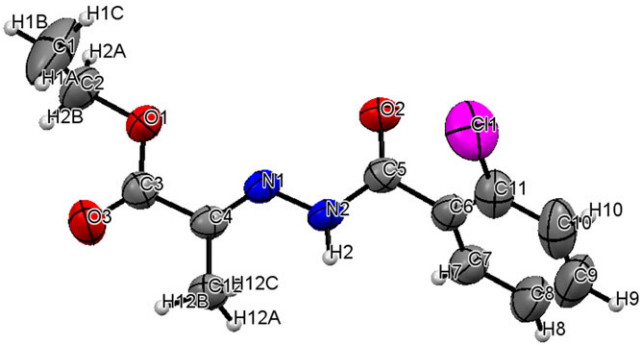

FIGURE 1 ORTEP diagram of ligand

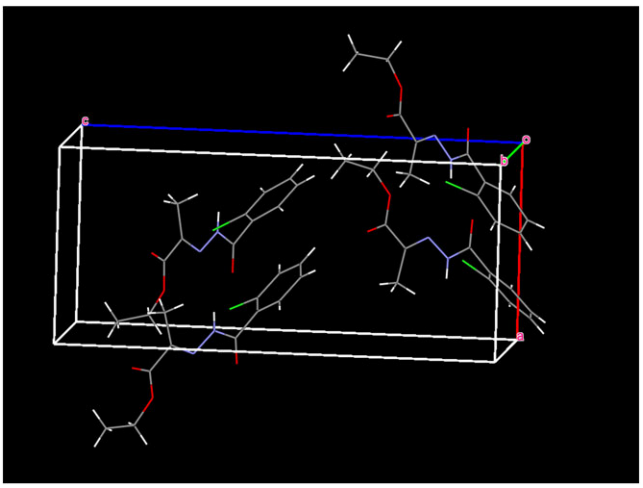

FIGURE 2 Packing diagram of ligand

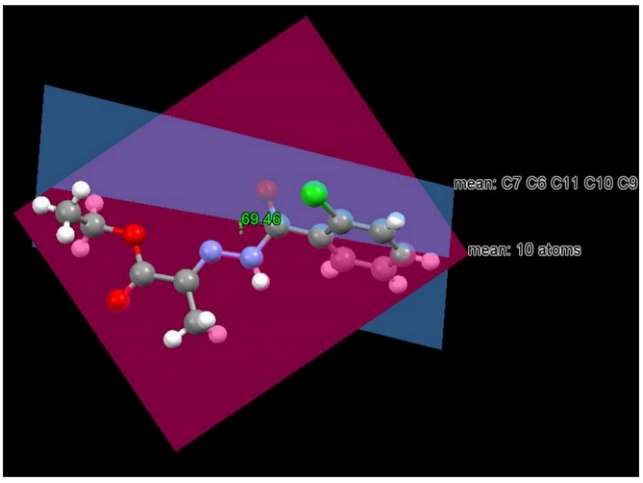

FIGURE 3 Possible planes in the ligand structure

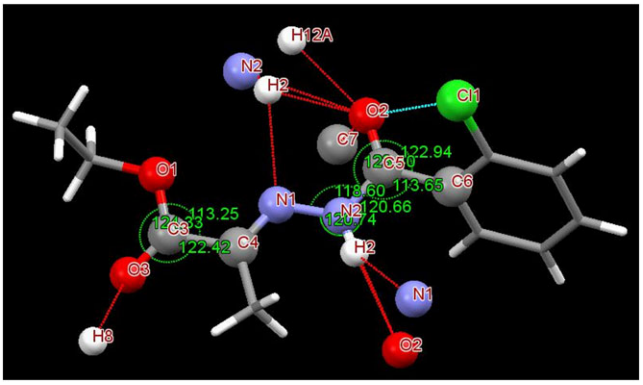

FIGURE 4 Intramolecular and intermolecular interactions in ligand structure

3.1 | Crystallographic study of ethyl 2-(2-(2-chlorobenzoyl)hydrazono)propanoate

The crystal structure refinement details, selected bond length and bond angles are presented in Tables 1–3 respectively. The ORTEP diagram, molecular packing diagram and molecular planes are presented in the Figures 1–3 respectively. The frames were integrated with the Bruker SAINT Software package using a narrow-frame algorithm. The single crystal X-ray diffraction of the new ligand was

TABLE 4 Diagnostic IR bands (cm^{-1}) of ligand and its metal complexes

Compound name	ν (C5 = O3) (amide)	ν (C3 = O2) (pyruvate)	ν (C3O2O1)		ν (C4 = N1)
			ν_{asym}(COO)	ν_{sym}(COO)	
L	1692	1717	----	----	1614
CoL	1649	Disappeared	1593	1376	1570
NiL	1620	Disappeared	1592	1384	1570
CuL	1647	Disappeared	1593	1383	1583
ZnL	1658	Disappeared	1597	1361	1570

TABLE 5 ^{1}H and ^{13}C NMR spectral data for ligand and its zinc complex (shifts in ppm)

Position	Ligand		Zn-complex	
	^{1}H–NMR	^{13}C–NMR	^{1}H–NMR	^{13}C–NMR
N2H	11.21 (s,1H)	-	11.20 (s,1H)	-
N2H′	11.47 (s,1H)	-	-	-
C1	1.26 (t,3H)	14.16	-	-
C1′	1.04 (t,3H)	13.89		
C2	4.22 (q,2H)	61.30	-	-
C2′	4.01 (q,2H)	60.82		
C3	-	170.38	-	174.66
C3′		170.32		-
C4	-	134.94	-	137.06
C4′		135.48	-	-
C5	-	164.67	-	166.81
C5′	-	163.80	-	-
C6	-	130.70	-	129.88
C6′	-	130.47	-	-
C7	7.38 (d,1H)	128.95	7.35 (t,1H)	130.20
C7′	7.38 (d,1H)	128.95	-	-
C8	7.43 (t,1H)	129.61	7.42(t,1H)	130.46
C8′	7.43 (t,1H)	129.61	-	-
C9	7.45 (t,1H)	131.61	7.45 (t,1H)	131.27
C9′	7.45 (t,1H)	131.61	-	-
C10	7.53 (d,1H)	127.23	7.63 (d,1H)	126.64
C10′	7.53 (d,1H)	126.72	-	-
C11	-	145.38	-	151.15
C11′	-	145.38	-	-
C12	2.48 (s,3H)	12.89	7.33 (s,3H)	12.30
C12′	2.48 (s,3H)	12.89	-	-

found to be orthorhombic having the space group *Pna* 21 with a = 8.31 Å, b = 8.51 Å, c = 18.59 Å, α = 90°, β = 90°, γ = 90°, V = 1317.34 Å^3 and Z = 4 for the formula $C_{12}H_{13}ClN_2O_3$.

The molecule shows two molecular planes having C6-C11 atoms in one plane and acetylhydrazonopropanoate part in another plane forming an angle 69.46° between the two planes. In this molecule amide carbonyl oxygen O2 is involved in intramolecular interaction with phenyl chlorine and intermolecular interactions with nitrogen N2, hydrogens H2, H12A and carbon C7 as shown in Figure 4. Because of these interactions the bond angle of N2-C5-C6 deviated from 120° to 113.65° and bond angle N1-N2-C5 reduced to 118.60°, it is further supported by the intermolecular interaction of N1 with H2 and involvement of hydrogen H2 bonded to N2 in intermolecular interaction with N1 and O2. The bond angle of O1-C3-C4 also deviates from 120° to 113.25° and is because oxygen O3 is involved in interaction with H8 of another molecule.

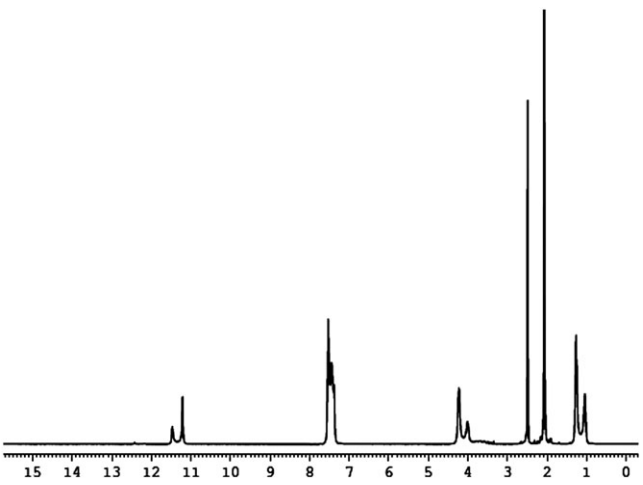

FIGURE 5 1H NMR spectrum of ligand

3.2 | Infrared spectral studies

The *insitu* convertion of ligand into its carboxylic acid and its further coordination to the metal ion can be supported by their IR spectral data. The diagnostic IR bands of ligand and its complexes are compiled in Table 4**.**

The strong band due to azomethine ν(C4=N1) functional group in the uncoordinated ligand was observed at 1614 cm^{-1} and has shifted to lower wave number ligand on complex formation, indicating the coordination of through azomethine nitrogen to the metal ion.[28] The strong band at 1717 cm^{-1} in ligand spectrum assigned to carbonyl ν(C3 = O2) stretching frequency has disappeared on complex formation. Simultaneously two new bands have appeared in the range of 1592–1597 cm^{-1} and 1361–1384 cm^{-1}, and were assigned to the respective asymmetric and symmetric

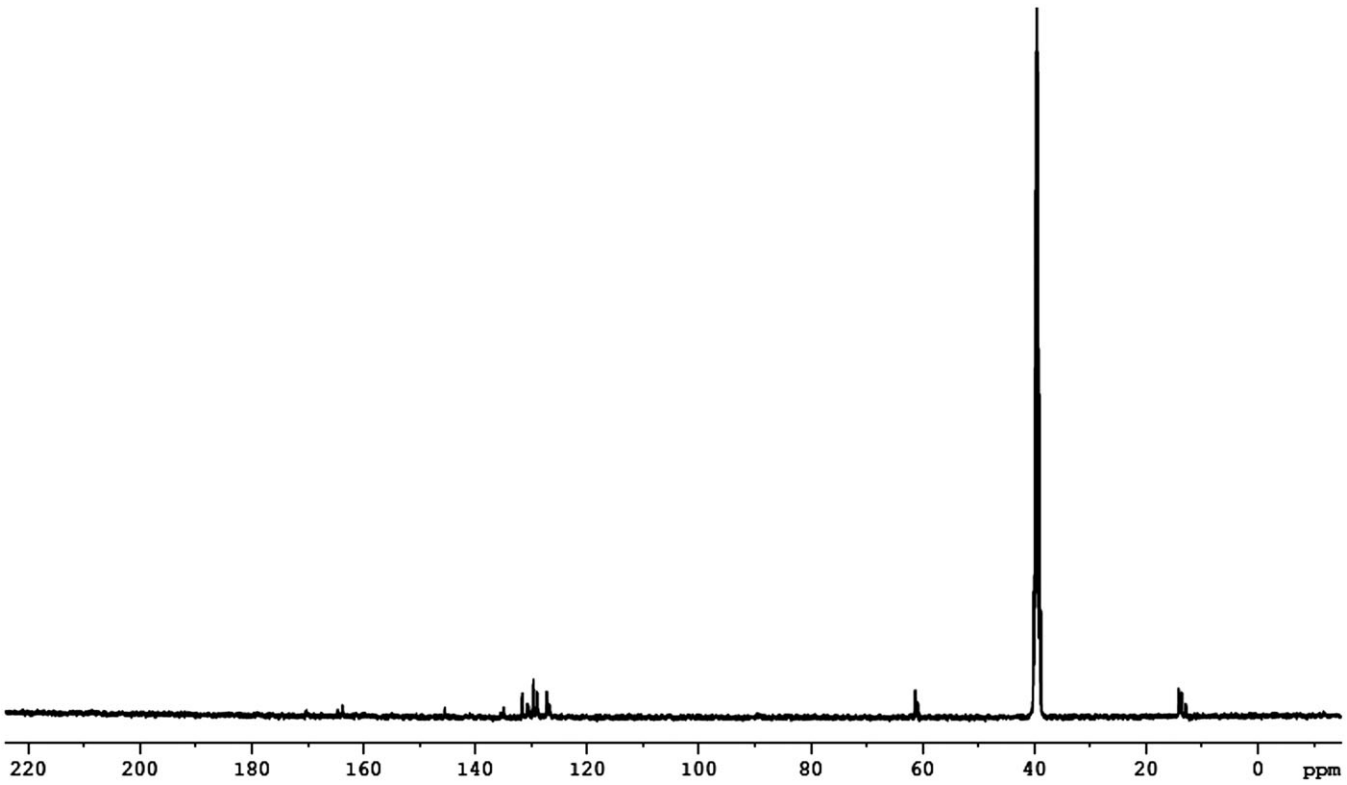

FIGURE 6 13C NMR spectrum for ligand

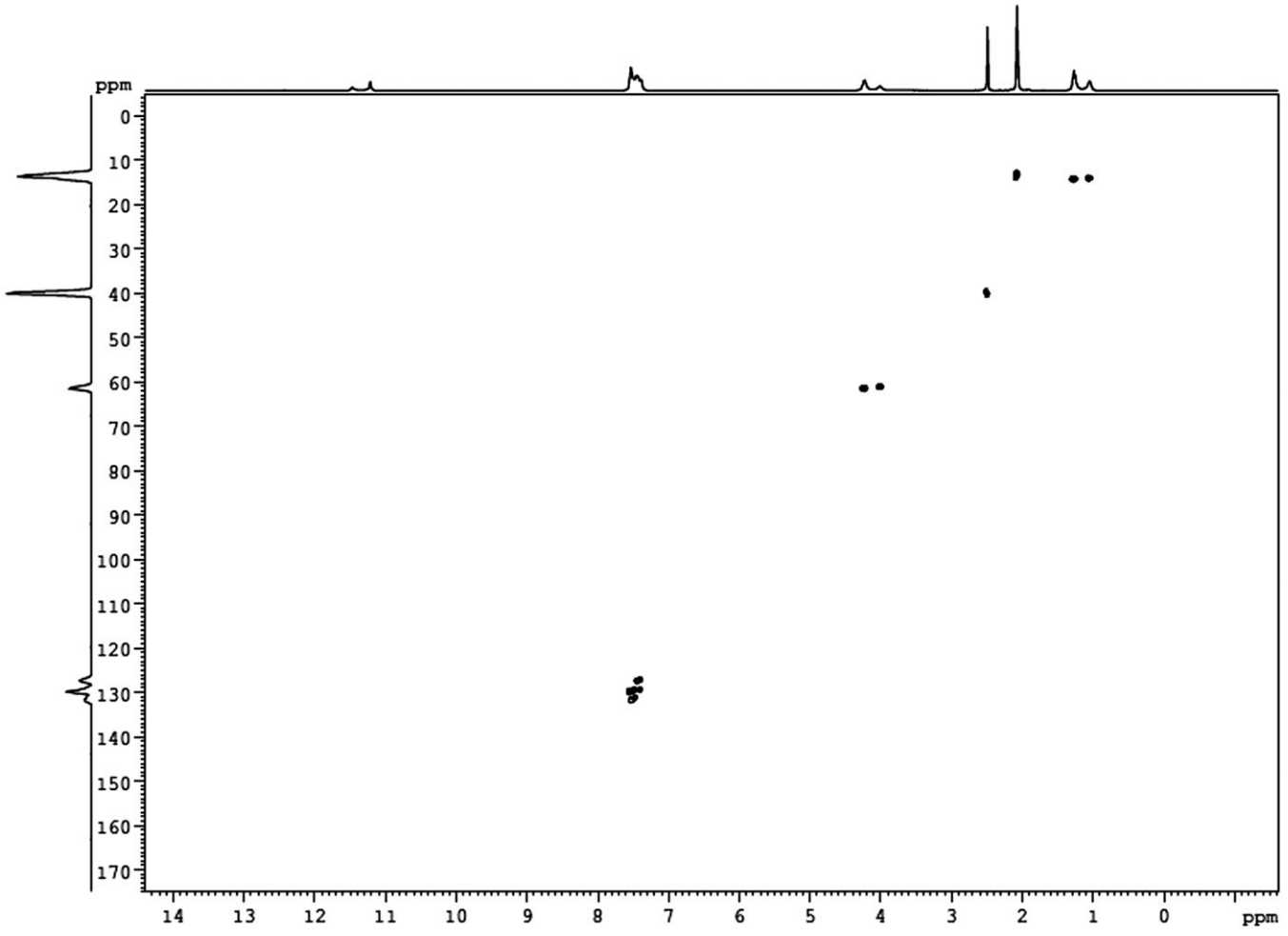

FIGURE 7 2D CH COSY NMR spectrum for ligand

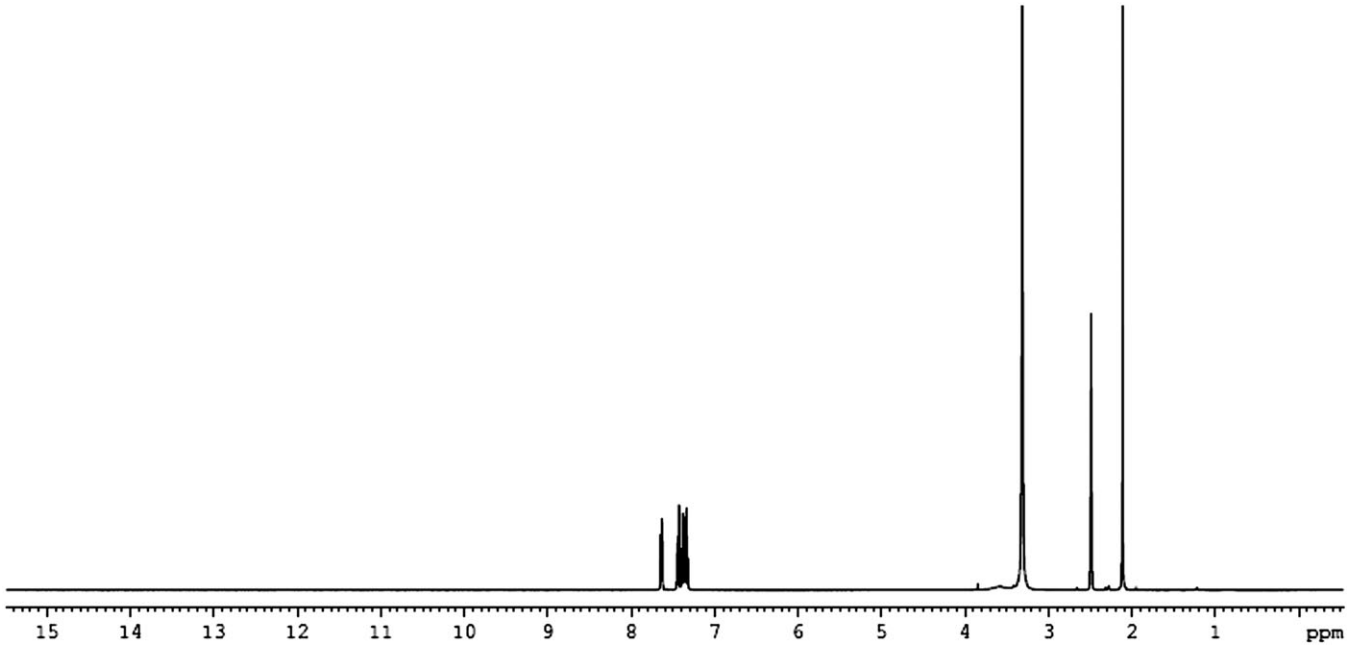

FIGURE 8 1H NMR spectrum for ZnL

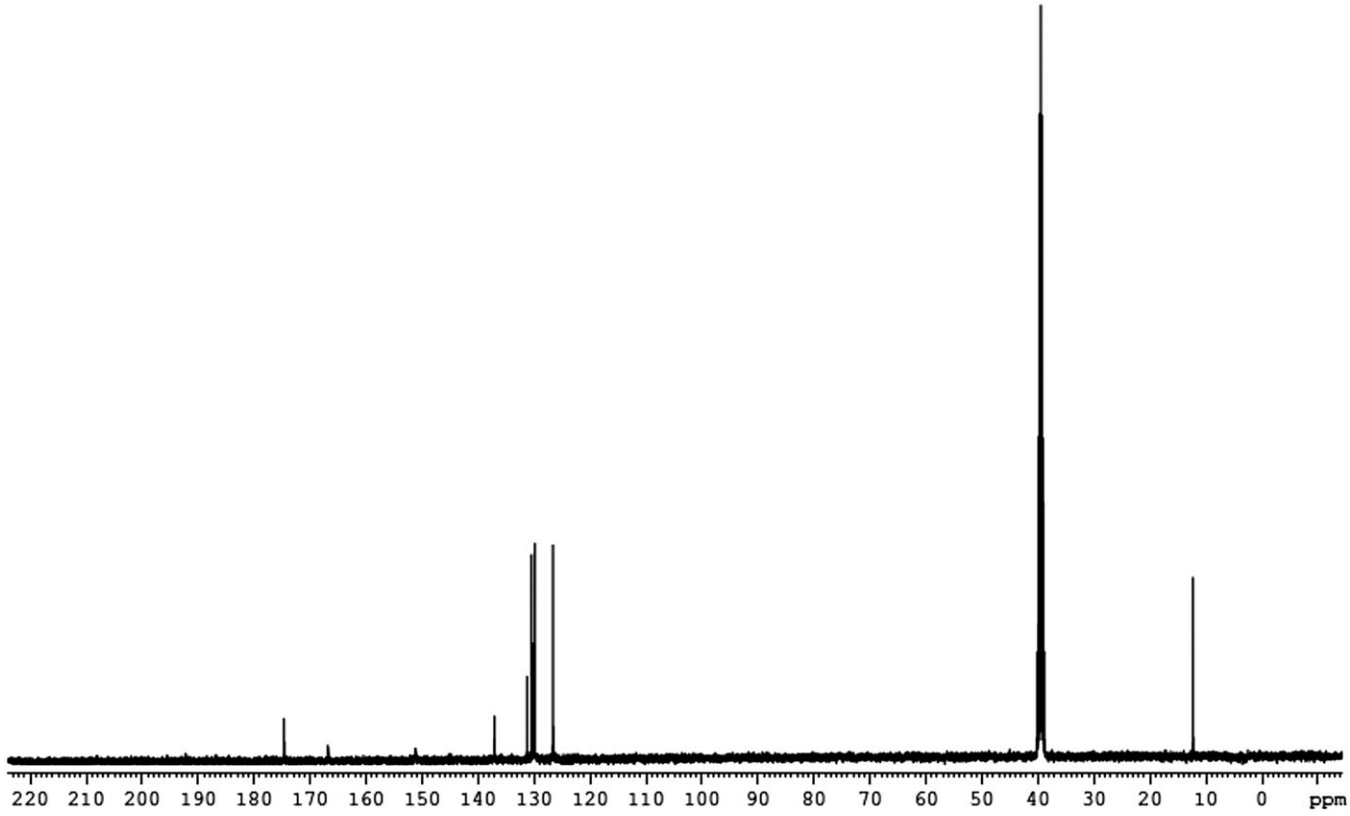

FIGURE 9 13C NMR spectrum for ZnL

stretching frequencies of coordinated carboxylate ion. This observation indicates that, the ester group of ligand was converted to carboxylic acid group before complex formation *in-situ* and the later same carboxylic acid moiety was involved in coordination to the metal ion. To confirm this phenomenon, the ligand was converted into sodium salt of its carboxylic acid by hydrolysis using NaOH and its IR spectrum was compared with the spectra of metal complexes. This suggests that, carboxylic acid has coordinated to metal ion. The difference between $\nu_{asym}(COO^-)$ and $\nu_{sym}(COO^-)$ frequencies in all complexes were found to be greater than the difference observed in the sodium salt of the ligand. This implies that, carboxylate group of ligand has coordinated to metal ion in unidentate fashion as suggested by Deacon.[29,30]

The amide carbonyl stretching frequency ν(C5 = O3) observed at 1692 cm^{-1} in ligand has shifted to 1649, 1620, 1647 and 1658 cm^{-1} in CoL, NiL, CuL and ZnL respectively suggesting the involvement of amide carbonyl oxygen in coordination. A sharp band of medium intensity in the ligand spectrum at 3194 cm^{-1} assigned ν(N2H) has remained unaltered/slightly changed in the spectra of complexes suggesting its non-involvement in the enolisation with adjacent carbonyl group. This was further confirmed by presence of N2H peak in ^{1}H NMR of zinc complex.

Thus, IR spectral analyses suggest the involvement of amide carbonyl oxygen, azomethine nitrogen and carboxylate oxygen in coordination and the ligand behaves as monobasic tridentate towards all the metal ions.

3.3 | NMR studies

The ^{1}H and ^{13}C NMR spectral assignments of ligand and its Zn(II) complex are compiled in Table 5**,** and the numbering scheme followed for the NMR assignment is presented in Scheme 1**.** The ^{1}H, ^{13}C and 2D CH COSY NMR spectra of ligand are depicted in Figures 5–7**,** and those of Zn (II) complex are presented in Figures 8–10**.**

The ligand has shown two set of signals in the ^{1}H, ^{13}C and 2D CH COSY NMR spectra which corresponds to its cis and trans isomeric forms aroused due to restricted rotation along N1 = C4 double bond. On complex formation, only one set of signals were observed indicating the presence of single form of ligand in the complex.[31,32]

The singlet at 11.21 ppm assigned to N2H proton has remained almost unaltered on complex formation, suggesting its noninvolvement in enolisation. The protons corresponding to C1 and C2 in ligand observed at 1.26/1.04 (t, 3H) and 4.22/4.01 (q, 2H) were absent in ^{1}H NMR spectrum of its zinc complex, suggesting its hydrolysis and formation of carboxylate ion. In ^{13}C NMR spectrum of the ligand, the signals due to C1 and C2 appeared at 14.16/13.89 and 61.30/60.82 ppm are absent in ^{13}C NMR spectrum of the zinc complex. This is further confirmed by 2D CH

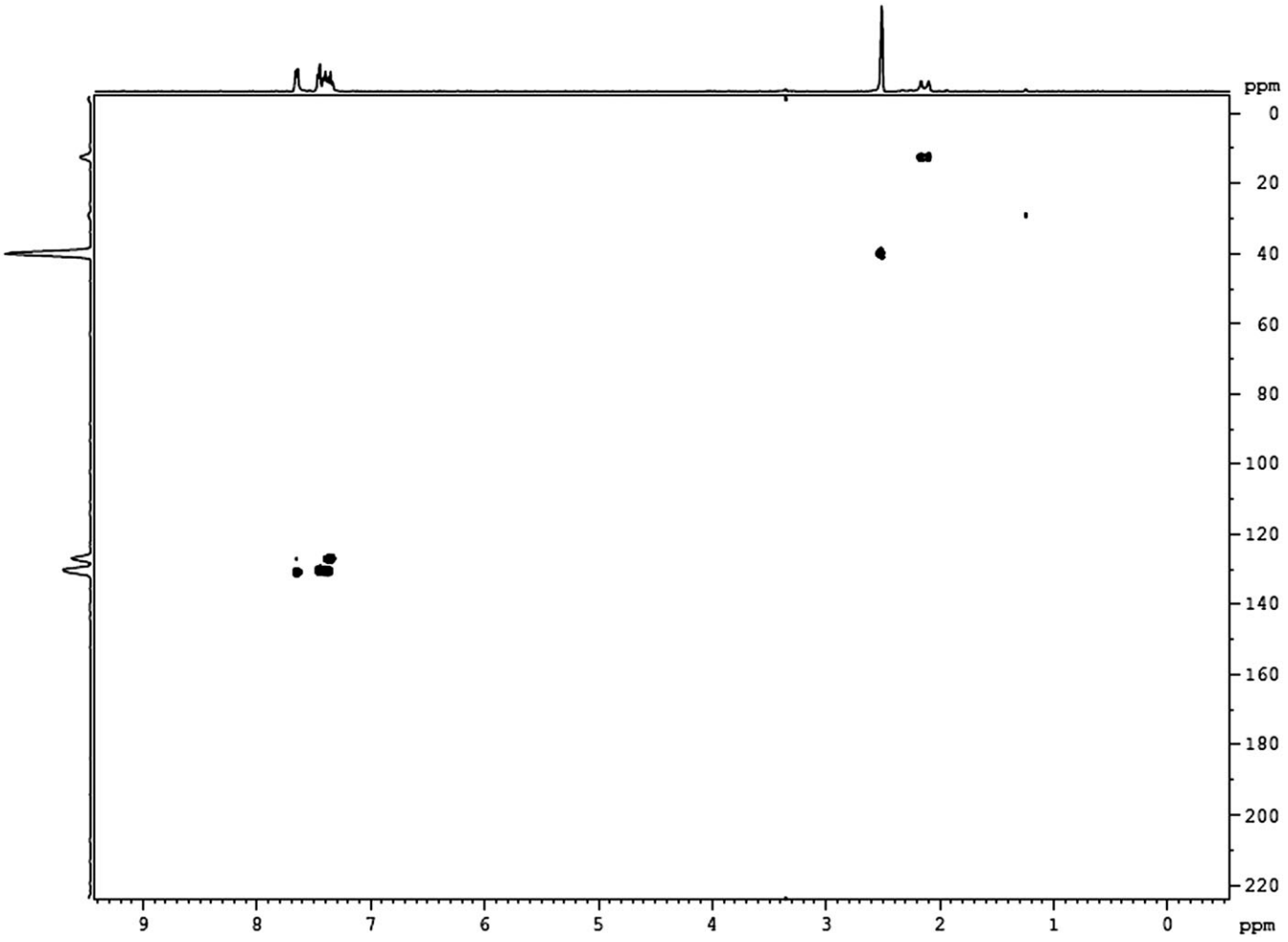

FIGURE 10 2D CH COSY NMR spectrum for ZnL

COSY NMR spectral study. The downfield shift of signals due to C3, C4 and C5 suggests the involvement of carboxylate oxygen, azomethine nitrogen and amide carbonyl oxygen of the ligand in coordination respectively with zinc (II).[33] The remaining signals are observed in the expected regions and confirm the structure of the ligand and its zinc complex.

3.4 | Electronic spectral studies of ligand and its complexes

Electronic spectra of ligand and their complexes were recorded in order to assign the plausible geometry around the metal ions. Representative electronic spectra of ligand and nickel complex are shown in Figures 11 and 12

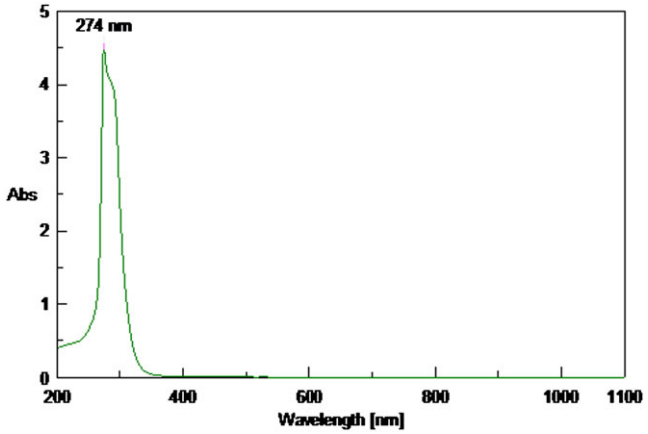

FIGURE 11 UV–visible spectrum of ligand

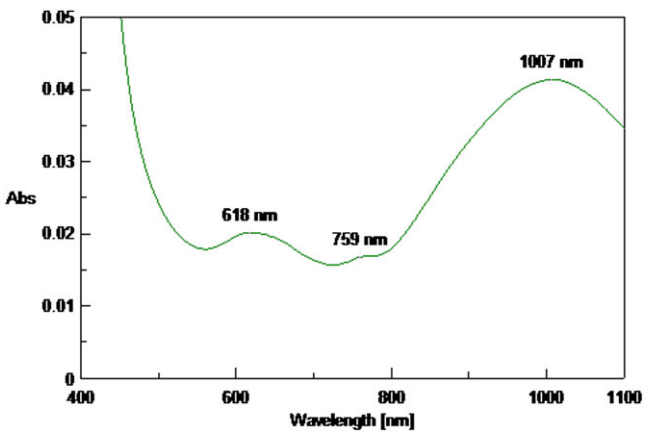

FIGURE 12 UV–visible spectrum of NiL

respectively. The band at 274 nm in the ligand spectrum is assigned to $\pi \rightarrow \pi^*$ transition. The cobalt complex shows a peak at 514 nm and was attributed to $^4T1g(F) \rightarrow {}^4T_{1g}(P)$, suggesting an octahedral structure. The bands at 618, 759 and 1007 nm in the spectrum of nickel(II) complex are assigned to $^3A_{2g}(F) \rightarrow {}^3T_{1g}(P)$, $^3A_{2g}(F) \rightarrow {}^3T_{1g}(F)$ and $^3A_{2g}(F) \rightarrow {}^3T_{2g}(F)$ suggesting octahedral geometry. The typical d-d absorption band due to $^2Eg \rightarrow {}^2T_{2g}$ was observed at 601 nm and is suggestive of a distorted octahedral structure for copper(II) complex.[34]

3.5 | Mass spectral studies of ligand and its complexes

The mass spectrum of ligand shows molecular ion peak at 269 (M^+) which corresponds to its molecular weight. The ESI mass spectra of cobalt, nickel, copper and zinc complexes show molecular ion peaks at m/z 537 $(M-1)^+$, 537 (M^+), 543 $(M + 1)^+$ and 544 (M^+) corresponding to their respective molecular weights. Mass spectrum of the ligand and ESI-mass spectra of cobalt complex are shown in

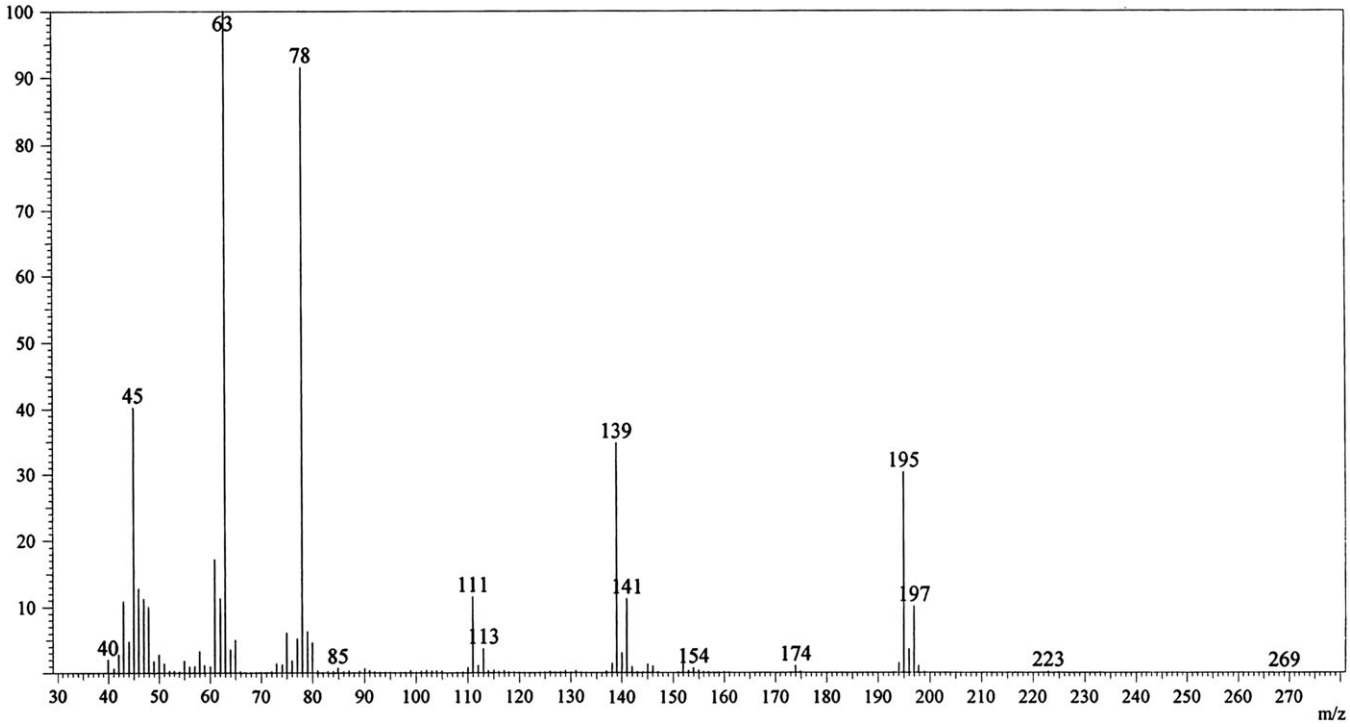

FIGURE 13 GC-mass spectrum for ligand

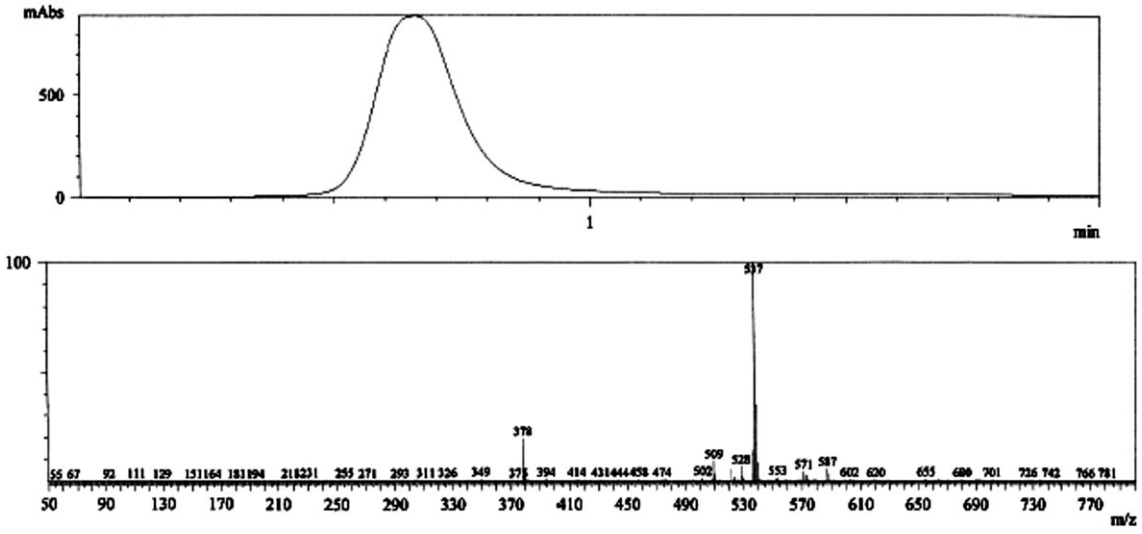

FIGURE 14 ESI mass spectrum of CoL

Figures 13, 14 respectively. (ESI-mass spectra of NiL and ZnL are shown in Figures S1-S2 respectively).

3.6 | Thermal studies of ligand and its complexes

In order to study the thermal stability and decomposition pattern, we have undertaken the thermogravimetric studies of all synthesized complexes in the temperature range 25–800 °C and decomposition details are presented in Table 6 and representative thermogram in Figure 15.

All the complexes exhibited a weight loss around 110 °C indicating the presence of lattice held water molecules. In the thermograms of CoL and NiL complexes, a weight loss in the range of 3.17–3.5% was observed between 70–105 °C and 75–120 °C respectively, suggesting presence of one lattice held water molecule. In case of CuL and ZnL complexes, weight loss of 6.14 to 6.11%, observed in the range of 68–108 °C and 75–110 °C corresponds to the loss of two lattice held water molecules.[35]

The loss of lattice held water molecules is followed by the loss of ligands in all the complexes. The weight loss of 85.98%, 85.99% and 82.71% in the temperature range of 105–631 °C, 120–628 °C and 108–568 °C assignable to the loss of two ligand in CoL, NiL and CuL complexes. But in ZnL, second step of weight loss of 82.38% is observed in the range 350–637 °C. The plateau obtained after the loss of ligand corresponds to the formation of metal residue.

3.7 | DNA binding studies

3.7.1 | Absorption spectral studies

Examining the changes in absorption spectrum of the metal complexes upon addition of increasing amounts of DNA is

TABLE 6 Thermal decomposition details of the complexes

Comp.	Temp. Range (in °C)	Weight loss in %		Weight loss due to
		Found	Calc.	
CoL	70–105	3.17	3.24	One lattice held water molecule
	105–631	85.98	86.35	Two ligands
	631–800	10.85	10.41	Metal residue
NiL	75–120	3.50	3.23	One lattice held water molecules
	120–628	85.99	86.20	Two ligands
	628–800	10.51	10.57	Metal residue
CuL	68–108	6.14	6.21	Two lattice held water molecules
	108–568	82.71	82.80	Two ligands
	568–800	11.15	10.99	Metal residue
ZnL	75–110	6.11	6.19	Two lattice held water molecules
	350–637	82.38	82.54	Two ligands
	637–800	11.51	11.27	Metal residue

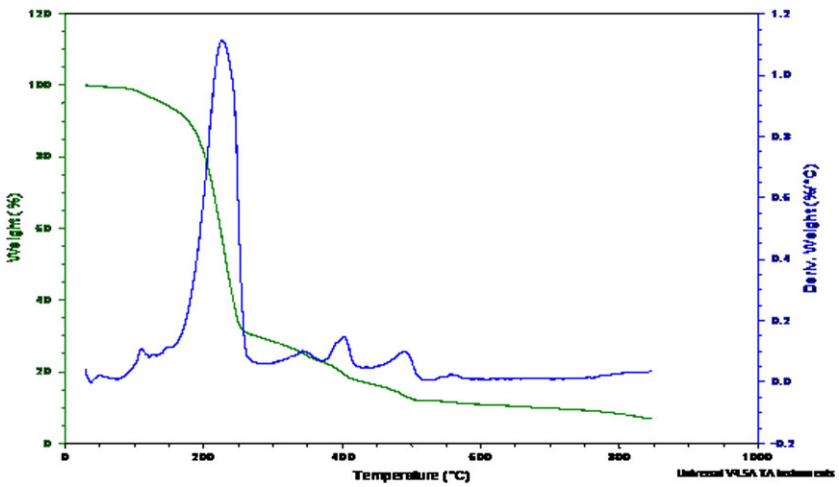

FIGURE 15 Thermogram for CuL

one of the most widely used methods to know the interaction of metal complexes with DNA and for determining overall binding constants. The absorption spectra of ligand and complexes in the presence and absence of CT-DNA are shown in the Figure 16**.** A complex binding to DNA through intercalation usually results in hypochromism and bathochromism involving strong stacking interaction between an aromatic chromophore and the base pairs of DNA. Upon addition of calf-thymus DNA to ligand and its complexes, there is a decrease in molar absorptivity (hypochromic shift) of the intense intraligand absorption bands (240–400 nm) of complexes. The hypochromic shift in case of ligand (264 nm), cobalt complex (268 nm), nickel complex (266 nm), copper complex (268 nm) and zinc complex (262 nm) is indicating strong binding of ligand and complexes with DNA. In order to compare the DNA-binding affinities of these complexes quantitatively, their intrinsic binding constants with CT-DNA were obtained by monitoring the changes in absorption at intraligand band with increasing concentrations of DNA using equation 1 and were found to be 0.97 x 10^4, 0.95 x 10^4, 0.75 x 10^4, 2.63 x 10^4 and 0.78 x 10^4 M^{-1} for ligand, cobalt, nickel, copper and zinc complexes respectively, indicating their binding interaction to DNA. Among all the compounds copper complex has shown a strong binding to DNA.

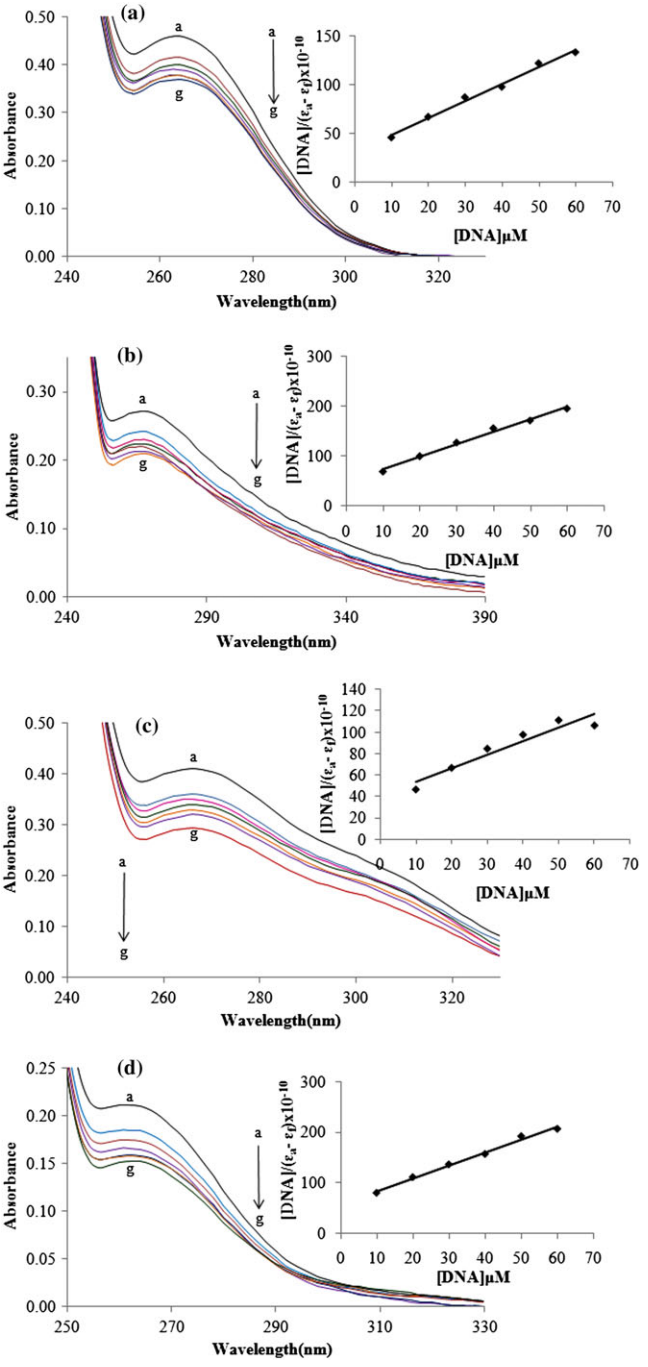

FIGURE 16 Changes in the electronic absorption spectra of L(a), CoL(B), NiL(C) and ZnL(D)(20uM) with increasing concentrations (0-50uM) of CT-DNA(phosphate buffer); the inset shows a fitting of the absorbance data at 264 nm for L, 268 nm for CoL, 266 nm for NiL and 262 nm for ZnL used to obtain binding constants

3.7.2 | DNA thermal denaturation

Interacalation of small molecules into the double helix is known to increase the helix melting temperature (Tm), the temperature at which the double helix denatures into single-stranded DNA. The extinction coefficient of DNA bases at 260 nm in the double strand is much less than that in the single-stranded form. Hence, melting of the helix leads to an increase in the absorption at this wavelength. *E. coli* DNA was seen to melt at 55–60 °C (phosphate buffer) in the absence of complex. The melting temperature of DNA for ligand, and nickel complex were found to be in the region 60–65 °C, for cobalt and zinc complexes it is found in the range 65–70 °C and for copper complex it is found in the region 70–75 °C (Figure S3). This indicates that copper complex bind strongly compared too other compoubnds tested. This behavior is comparable to classical intercalators.[36]

3.7.3 | Ethidium bromide displacement assay

The competitive DNA binding of complexes has been studied by examining changes in emission intensity of ethidium bromide (EtBr) bound to CT-DNA as a function of added complex concentration.[37] Though the emission intensity of EtBr in buffer medium is quenched by the solvent molecules, it is enhanced by its stacking interaction between adjacent DNA base pairs. When ligand and complexes were added to DNA pretreated with EtBr {[DNA]/[EtBr] = 1:1}, the DNA-induced emission intensity of EtBr has decreased (Figure 17). The Kapp values 5.00x10^6 M^{-1} for ligand, 6.66x10^6 M^{-1} for CoL, NiL, 10.00x10^6 M^{-1} for CuL and 4.00x10^6 M^{-1} for ZnL. The higher values of Kapp indicate that these complexes bind to DNA by intercalation.

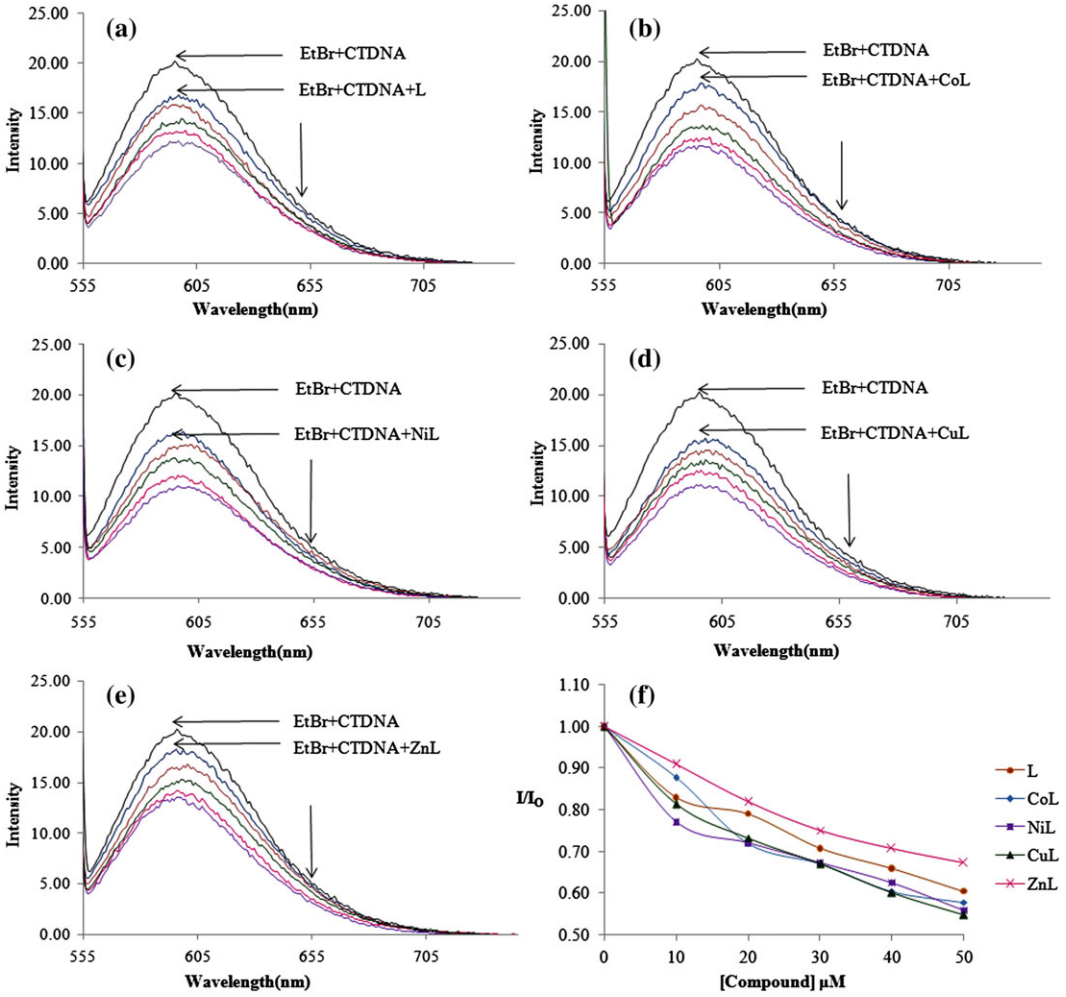

FIGURE 17 Effect of addition of L(a), CoL(B), NiL(C), CuL(D), ZnL(E) on the emission intensity of the CT-DNA bound ethidium bromide (20uM) at different concentrations in phosphate buffer(pH = 7.2). (F) plots of relative integrated emission intensity versus [DNA]/[compound] for LH, col, nil, CuL and ZnL

3.7.4 | Viscosity measurements

Absorption and emission studies generally provide necessary, but not sufficient clues to support interacalative binding mode. To further clarify the nature of the interaction between the complexes and DNA, viscosity measurements were carried out. Hydrodynamic measurements are sensitive to change in length of DNA and considered to be the most critical and least ambiguous tests in evaluating binding modes in solution in the absence of crystallographic structural data. Lengthening of DNA helix occurs on intercalation as base pairs are separated to accommodate the binding ligand leading to increase in DNA viscosity.[38] Partial or on classical intercalation of ligand may bend or kink the DNA helix, thereby decreasing its effective length and subsequently viscosity. The values of relative specific viscosities of DNA in the absence and presence of complexes are plotted against [complex]/[DNA]. The relative viscosities of CT-DNA bound to ligand and its complexes have increased with

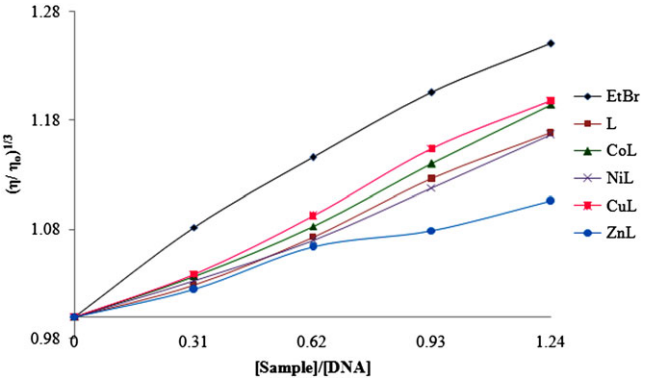

FIGURE 18 Effect of increasing amount of the EtBr, L, CoL, NiL, CuL and ZnL on the relative viscosities of CT-DNA at 28 °C, [DNA] = 200uM. The results are the mean of three independent experiments carried out under identical conditions

increasing concentration (Figure 18).similar to some known intercalators, indicative of a classical intercalation.[39]

3.7.5 | DNA cleavage studies

Many studies have shown that the clinical efficacies of many drugs correlate with their ability to induce DNA cleavage. The extent to which the newly synthesized ligands and their metal complexes could function as DNA cleavage agents is examined using supercoiled (SC) plasmid pBR322 DNA as a target. The agarose gel electrophoresis method is employed to study the efficiency of cleavage by the synthesized compounds. The photograph representing the cleavage of DNA by various samples is presented in Figure 19.

The characterization of DNA recognition by transition metal complex has been aided by the DNA cleavage chemistry that is associated with redox-active or photoactivated metal complexes. The electrophoretic analysis clearly reveals that the new molecule and their metal complexes have acted on DNA as there has been a difference in molecular weight between the control and the treated DNA samples. Usually the pBR 322 plasmid shows nicked/open circular, linear and supercoiled DNA bands.[40,41] It is observed that at a given concentration, there is diminishing of bands with a prominent streak indicating more cleavage activity of copper complex. But the ligand, cobalt, nickel and zinc complexes are not showing significant cleavage of bands.

3.8 | Anticancer studies

3.8.1 | MTT assay

The anticancer activities of ligand, and its copper complex were screened for their *in vitro* cytotoxicity against KB (Oral), A431 (Skin), MIA-Pa-Ca (Pancreases), K-549 (Lung), K-562 (Leukemia), MCF-7 (Breast) and VERO cell lines, to obtain information about the anticancer potential of the newly synthesized compounds. The results suggest that the compounds exhibit good cytotoxic activities in a concentration dependent manner. Cisplatin was used as reference drug. The cytotoxicity activities of the most potent derivatives were also tested in MCF-7, KB, A431, Mia-Pa-Ca-2, K-562 cell lines and were treated with different concentrations of each compound for 72 h and it was observed that all compounds prevent cell growth in a dose dependent manner. The IC_{50} values (concentration that inhibits 50% of cell growth) for all compounds were determined by 3-(4,5-Dimethylthiazol-2-yl)-2,5-Diphenyltetrazolium Bromide (MTT).

As shown in **Graphs 1** to **6**, copper complex exhibited enhanced cytotoxic activity with all the six cell lines

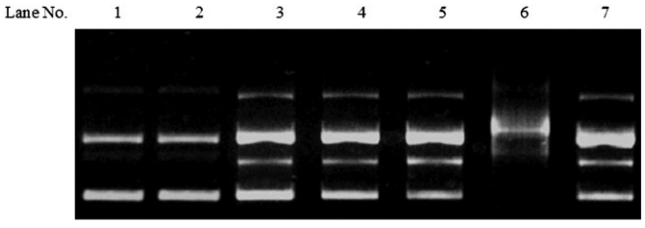

FIGURE 19 Lane 1, DNA control; Lane2, DNA+ solvent; Lane3, DNA + L(100uM); Lane4, DNA + CoL (100uM); Lane5, DNA + NiL(100uM); Lane6, DNA + CuL(100uM); Lane7, DNA + ZnL(100uM). Graphic 1. Cytotoxicity against oral cancer cell lines(KB). Graphic 2. Cytotoxicity against Skin cancer cell lines (A431). Graphic 3. Cytotoxicity against pancreas cancer cell lines (MIAPACA). Graphic 4. Cytotoxicity against Lung cancer cell lines (A549). Graphic 5. Cytotoxicity against Leukemia cell lines (K562). Graphic 6 cytotoxicity against Breast cancer cell line (MCF-7)

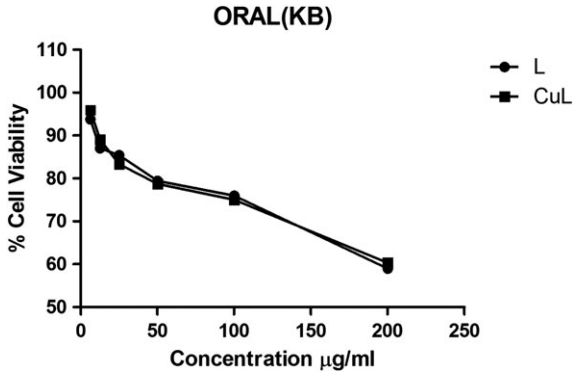

GRAPH 1 Cytotoxicity against Oral cancer cell lines(KB)

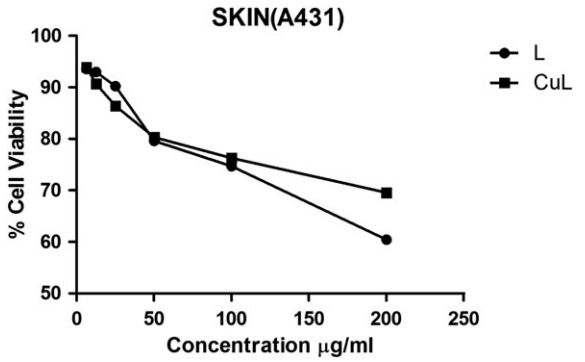

GRAPH 2 Cytotoxicity against Skin cancer cell lines (A431)

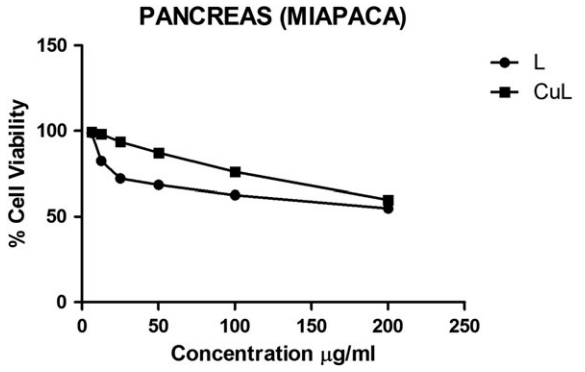

GRAPH 3 Cytotoxicity against Pancreas cancer cell lines (MIAPACA)

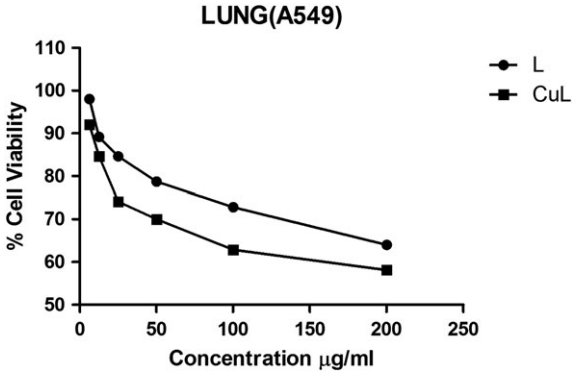

GRAPH 4 Cytotoxicity against Lung cancer cell lines (A549)

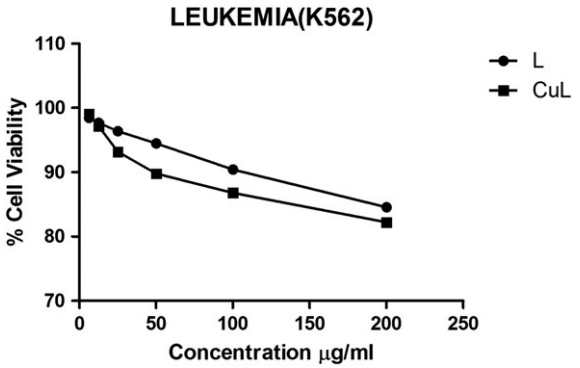

GRAPH 5 Cytotoxicity against Leukemia cell lines (K562)

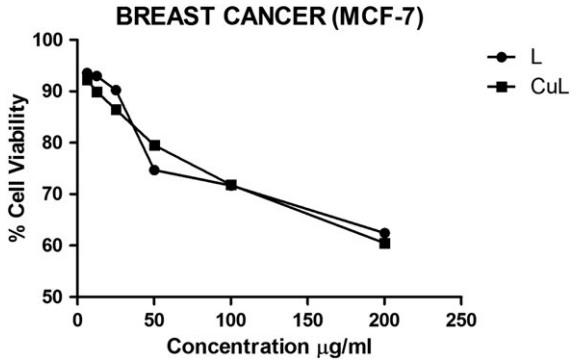

GRAPH 6 Cytotoxicity against Breast cancer cell line (MCF-7)

compared to ligand alone. In this case, the enhancement of antiproliferative activity, with respect to other compounds, might be related to their different structural characteristics and mainly attributed to redox active metal ion and the attached ligand. The antiproliferative activity of both ligand and copper complex on tested cell lines are in the order KB > A-431 > Mia-Pa-Ca > A-549 > K-562 > MCF-7 > VERO. The cytotoxicity of these compounds on VERO cell line showed IC_{50} value 560 µg/ml, which suggest that these compounds have a low toxicity to VERO cell lines. The IC_{50} values are compared between L and CuL for their action on KB (Oral), A431 (Skin), MIA-Pa-Ca (Pancreases), K-549 (Lung), K-562 (Leukemia), MCF-7 (Breast) and VERO cell lines and are compiled in Table 7.

While tumor cells undergo apoptosis in the presence of anticancer drugs, normal cells become necrotic if the drug is toxic. MTT assays cannot differentiate between these mechanisms of cell death. Therefore, the effects of drug may primarily be toxic, poisoning normal cells. These drugs have limited clinical application. Therefore, detection of tumor cell apoptosis is more valuable than generally assessing tumor cell viability. Cisplatin in the treatment of human cancers as one of the most active chemotherapeutic drugs, was designated as a positive control.

3.8.2 | Acridine orange ethidium bromide (AO/EB) staining

KB, the oral cell line was labeled by AO/EB. Dual staining was examined under a fluorescent microscope. No significant apoptosis was detected in the negative control group. Primary stage apoptotic cells, marked by granular yellow green AO nuclear staining, were noticed in the experimental group. In ligand treated group the numbers of primary stage apoptotic cells were increased with increasing concentrations and treatment period. In the CuL treated cells, the apoptotic cells at final stage were also detected with rising concentration and period of treatment by EB stain which showed localized orange nuclear cells. Thus, results depicted raise in necrotic cells and exhibited uneven orange-red fluorescence at their periphery. Double AO/EB fluorescent staining can detect basic morphological changes in apoptotic cells. In addition, it permits to distinguish between normal, primary, late apoptotic and necrotic cells. Morphological evidence of apoptosis by AO/EB dual staining in L and CuL treated cells are shown in Figure 20.

TABLE 7 IC_{50} values of L, CuL and cisplatin (µg/ml)

Compound	KB	A431	MIAPACA	A549	K-562	MCF-7	Vero
L	5.42	4.55	15.19	50.65	168.84	4.31	562.82
CuL	2.14	1.49	4.98	16.60	55.35	2.24	184.50
Cisplatin	4.2	5.2	4.2	6.4	5.2	4.8	6.8

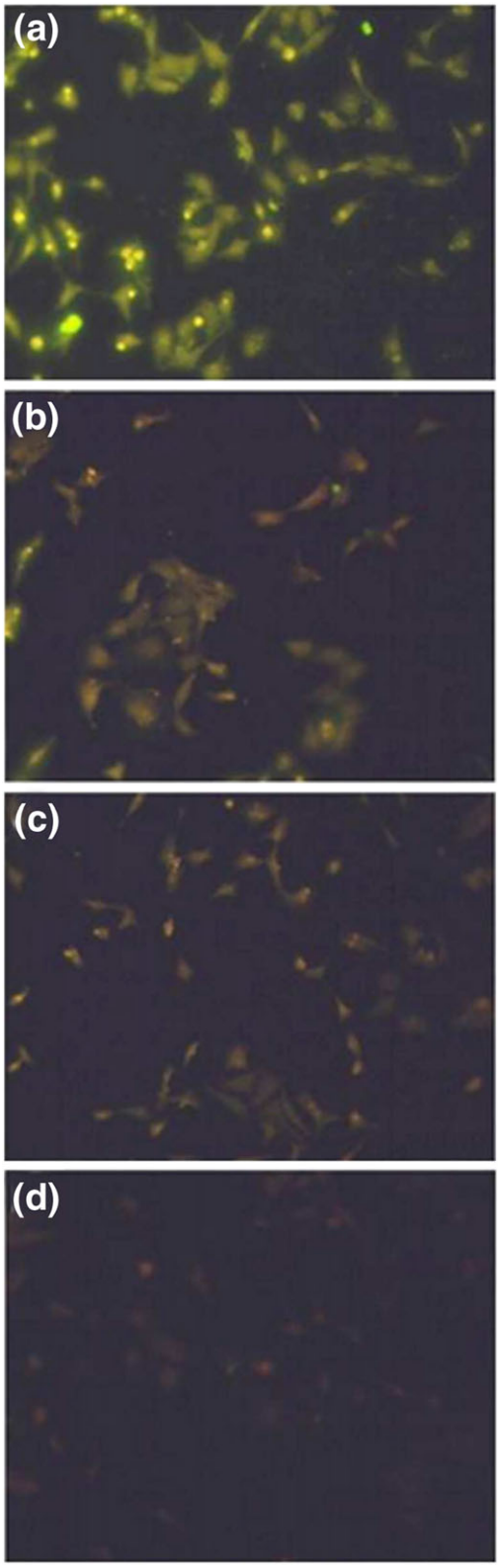

FIGURE 20 Morphological evidence of apoptosis by AO/EB dual staining L, CuL and. Cisplatin. (a) negative control group (untreated cells)-the circular nucleus homogeneously spread in the central region of the cell. (b) ligand treated cells showing early stage of apoptosis i.E cell shrinkage (c) positive control, cisplatin treated cells showing tigtly packed cells undergoing apoptosis. (d) CuL treated cells showing intense cell shrinkage showing strong apoptosis

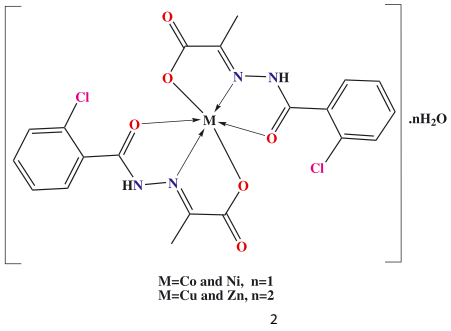

FIGURE 21 Tentative structures for the complexes

We guess that AO entered normal and primary apoptotic cells without damaging membranes, fluorescing green when attached to DNA. EB only entered cells with broken membranes, such as final stage apoptotic and deceased cells, radiating orange-red fluorescence when bound to concentrated DNA fragment or apoptotic forms.[42,43] Likewise, double AO/EB staining is capable to detect minor DNA damages. Hence, to distinguish normal, primary apoptotic, late apoptotic cells and the dead cells, nuclear morphology must be assessed. Fluorescent staining using Acridine Orange alone has been used earlier; though, revealing of cell apoptosis using AO/EB doubled staining is a comparatively different method, and very few articles have stated its usage.[44] In contrast to Acridine orange staining, the combined AO/EB method increases the rate of detection of apoptosis and can distinguish between different stages of apoptosis.

4 | CONCLUSION

The transition metal complexes of novel ligand ethyl-2-(2-(2-chlorobenzoyl)hydrazono)propanoate were synthesized and characterized using various physico-chemical techniques. The ligand behaves as a monobasic tridentate ligand with ONO donor sites. Elemental analyses, thermal and spectral studies confirm the proposed composition of metal complexes. The octahedral geometry was assigned for all the complexes and tentative structures proposed for them are presented in Figure 21. The strong ability of copper complex to bind to DNA (CT-DNA) has been suggested by absorption, emission, viscosity and thermal denaturation studies with *E. coli* DNA. The gel electrophoresis method confirms the higher ability of copper complex to cleave pBR322 DNA. The anticancer studies suggest that the cytotoxic activity of ligand was enhanced on formation of copper complex towards KB, MCF-7, A-431, Mia-Pa-Ca-2, A-549 K-562 and VERO cell lines. Copper complex has shown better activity against KB, A431 and MCF-7 cell lines compared to the standard used.

ACKNOWLEDGEMENT

The authors thank the USIC, Karnatak University, Dharwad for providing the spectral facilities and thankful to UGC for providing UGC-UPE fellowship and UPE-FAR-I program. Authors are thankful to Dr. V. Shyamkumar and Delicia A. Baretto for their support in conducting gel electrophoresis experiment.

REFERENCES

[1] B. W. Stewart, C. W. Wild, *World Cancer Report*, IARC Nonserial Publication, Stewart **2014**.

[2] *Global Cancer Facts & Figures*, 3rd ed., American Cancer Society **2015** 1.

[3] M. Dietel, *Targeted Therapies in Cancer*, **2007** 262.

[4] E. G. Mayer, *Principles of Anticancer Drug Development*, **2010** 674.

[5] P. C. Brooks, D. Morais, L. Liebes, D. Rodriguez, US 2005/0209334 A1, **2005**.

[6] R. Venkataraman, J. A. Kellum, M. Song, M. P. Fink, *Shock* **2002**, *18*, 507.

[7] H. Sabine, V. Rijt, P. J. Sadler, *Drug Discovery Today*, **2009** 14, 23.

[8] W. Zhao, G. G. Mackenzie, O. T. Murray, Z. Zhang, B. Rigas, *Carcinogenesis* **2009**, *30*, 512.

[9] S. Joseph, T. Nie, L. Huang, H. Zhou, K. Atmakur, R. C. Gupta, F. Johnso, B. Rigas, *Mol. Med. Rep.* **2011**, *4*, 891.

[10] M. P. Fink, *J. Intern. Med.* **2007**, *261*, 349.

[11] L. Ulloa, M. Ochani, H. Yang, M. Tanovic, D. Halperin, R. Yang, *Proc. Natl. Acad. Sci.* **2002**, *99*.

[12] M. Wang, L. F. Wang, Y. Z. Li, Q. X. Li, Z. D. Xu, D. M. Qu, *Transition Met. Chem.* **2001**, *26*, 307.

[13] M. B. Baile, N. S. Kolhe, P. P. Deotarse, A. S. Jain, A. A. Kulkarni, *International Journal of Pharma Research & Review* **2015**, *4*.

[14] P. Sathyadevi, P. Krishnamoorthy, R. R. Butorac, A. H. Cowley, N. Dharmaraj, *Metallomics* **2012**, *4*.

[15] M. Alagesan, N. S. P. Bhuvanesh, N. Dharamaraj, *Dalton Trans.* **2013**, *42*.

[16] P. Krishnamoorthy, P. Sathyadevi, R. R. Butorac, A. H. Cowley, N. S. P. Bhuvanesh, N. Dharmaraj, *Dalton Trans.* **2012**, *41*, 4423.

[17] A. Manvar, A. Malde, J. Verma, V. Virsodia, A. Mishra, K. Upadhyay, H. Acharya, E. Coutinho, A. Shah, *Eur. J. Med.Chem.* **2008**, *43*, 2395.

[18] G. M. Sheldrick, Shelxtl. Version 5.0 Bruker AXS Inc., Madison, WI, USA. **2001**.

[19] L. J. Farrugia, G. X. WinGX 1.64, *J. Appl. Crystallogr.* **1999**, 832.

[20] L. J. Farrugia, *J. Appl. Crystallogr.* **1997**, *30*, 565.

[21] A. H. Pathan, G. N. Naik, R. P. Bakale, S. S. Machakanur, K. B. Gudasi, *Appl. Organomet. Chem.* **2012**, *26*, 148.

[22] S. S. Bhat, A. A. Kumbhar, H. Heptullah, A. A. Khan, V. V. Gobre, S. P. Gejji, V. G. Puranik, *Inorg. Chem.* **2011**, *50*, 545.

[23] M. N. Patel, P. A. Dosi, B. S. Bhatt, *Appl. Organomet. Chem.* **2011**, *25*, 653.

[24] R. P. Reddy, R. Nomula, R. Pallepogu, H. Shaik, *Eur. J. Med. Chem.* **2014**, *79*, 117.

[25] A. Barve, A. Kumbhar, M. Bhat, B. Joshi, R. Butcher, U. Sonawane, R. Joshi, *Inorg. Chem.* **2009**, *48*, 9120.

[26] A. Dolly, J. B. Griffiths, *Cell And Tissue Culture For Medical Research*, **2000**

[27] I. C. Gherghi, S. T. Girousi, A. N. Voulgaropoulos, R. T. Tsitouridou, *Talanta* **2003**, *61*, 103.

[28] L. J. Bellamy, *The Infrared Spectra of Complex Molecules*, Methuen, London **1958** 353.

[29] G. B. Deacon, R. J. Philips, *Coord. Chem. Rev.* **1980**, *33*, 227.

[30] Nakamoto, *Infra-red and raman spectra of Complexes Inorganic and coordination Compounds, Part B*, John Wiley & Sons, New York, NY **1997**.

[31] M. Thomas, M. K. M. Nair, R. K. Radhakrishnan, *Synth. React. Inorg. Met. Org. Chem.* **1995**, *25*, 471.

[32] R. R. Gardner, S. L. McKay, S. H. Gellman, *Org. Lett.* **2000**, *2*, 2335.

[33] D. L. Pavia, G. M. Lampman, G. S. Krizand, J. R. Vyvyan, *Spectroscopy*. **2007**.

[34] D. N. Satyanarayana, *Electronic Absorption Spectroscopy and Related Techniques*. **2001**.

[35] Skoog, Holler, Crouch, *Instrumental analysis* **2003**. B. Yan, H. J. Zhang, G. L. Zhou, J. Z. Ni, *Chem. Pap.* **2003**, (57), 83.

[36] V. Rajendran, R. Karthik, M. Palaniandavar, H. S. Evans, V. S. Periswamy, M. A. Akbarsh, B. S. Srinag, H. Krishnamurthy, *Inorg. Chem.* **2007**, *46*, 8208.

[37] M. Lee, A. L. Rhodes, M. D. Wyatt, S. Forrow, J. A. Hartley, *Biochemistry* **1993**, *2*, 4237.

[38] L. Xiao-Wen, Z. Yong-Jun, L. Yan-Tuan, W. Zhi-Yong, Y. Cui-Wei, *Eur. J. Med. Chem.* **2011**, *46*, 3851.

[39] C. V. Kumar, E. H. Asunction, *J. Am. Chem. Soc.* **1993**, *115*, 8547.

[40] Y. Li, Y. Wu, J. Zhao, P. Yang, *J. Inorg. Biochem.* **2007**, *101*, 283.

[41] V. Uma, M. Kanthimathi, T. Weyhermuller, B. U. Nair, *J. Inorg. Biochem.* **2005**, *99*, 2299.

[42] H. Lecoeur, *Exp. Cell Res.* **2002**, *277*, 1.

[43] W. L. Biffl, E. E. Moore, F. A. Moore, C. C. Barnett, *J. Trauma Injury Infect Crit Care* **1996**, *40*, 575.

[44] D. Ribble, N. B. Goldstein, D. A. Norris, Y. G. Shellman, *BMC Biotechnol.* **2005**, *5*, 12.

SUPPORTING INFORMATION

Additional Supporting Information may be found online in the supporting information tab for this article.

How to cite this article: Hegde D, Dodamani S, Kumbar V, Jalalpure S, Gudasi KB. Synthesis, crystal structure, DNA interaction and anticancer evaluation of pyruvic acid derived hydrazone and its transition metal complexes. *Appl Organometal Chem*. 2017; e3851. https://doi.org/10.1002/aoc.3851